Extended Specifications and Test Data Sets for Data Level Comparisons of Direct Volume Rendering Algorithms

Kwansik Kim[1], Craig M. Wittenbrink[2] and Alex Pang[1,2]

[1] Computer Science Department

University of California, Santa Cruz

[2] Hewlett-Packard Laboratories

Palo Alto, California

March 12, 2001

Abstract

Direct volume rendering (DVR) algorithms do not generate intermediate geometry to create a visualization. Yet, they produce countless variations in the resulting images. Therefore, comparative studies are essential for objective interpretation. Even though image and data level comparison metrics are available, it is still difficult to compare results because of the numerous rendering parameters and algorithm specifications involved. Most of the previous comparison methods use information from final rendered images only. We overcome limitations of image level comparisons with our data level approach using intermediate rendering information. We provide a list of rendering parameters and algorithm specifications to guide comparison studies. We extend Williams and Uselton's rendering parameter list with algorithm specification items and provide guidance on how to compare algorithms. Real data are often too complex to

study algorithm variations with confidence. Most of the analytic test data sets reported are often useful only for a limited feature of DVR algorithms. We provide simple and easily reproducible test data sets, a checkerboard and a ramp, that can make clear differences in a wide range of algorithm variations. With data level metrics, our test data sets make it possible to perform detailed comparison studies. A number of examples illustrate how to use these tools.

Keywords and Phrases: Metrics, opacity, gradient, surface classification, volume visualization, image quality, uncertainty visualization.

1 Introduction

Objective comparison methods for algorithms are important in scientific visualization. Globus and Uselton [6] argued that it is necessary to distinguish artifacts generated in the visualization pipeline from the data features. Image metrics have been developed as quality measures, but, unlike other fields, comparison studies of the quality and accuracy of scientific visualization methods have only recently started. The varying quality and accuracy of visualizations can be attributed to a number of factors including uncertainty in the data gathering and modeling processes, data derivation and transformation stages, and in the data visualization process itself as pointed out by Pang et al. [22]. Klir [10] refines this by pointing out that uncertainty itself has many forms and dimensions and may include concepts such as fuzziness or vagueness, disagreement and conflicts, and imprecision and non-specificity. Since this paper is concerned with comparisons, uncertainty refers to differences arising from disagreement between two methods or sets of parameters.

Direct volume rendering, or DVR, is one of the most popular methods in visualizing 3D scalar fields. Some of the fundamental work can be found in Drebin et al. [4] and Levoy [13]. These have led to a number of different implementations some of which we examine in this paper. They include splatting reported in Westover [27, 28] and Laur and Hanrahan [12], projection based algorithms such as those by Wilhelms and Van Gelder [29] and Williams and Max [30], and speed

optimizations such as Lacroute and Levoy's shear-warp [11] and volume texture map techniques proposed by Cabral et al. [3] and Van Gelder and Kim [25]. As is well known, each DVR method produces somewhat different images. The rendering parameter and algorithm settings are often dependent on the application domain. For example, proper settings for data from computational fluid dynamics field are often inappropriate for data from medical imaging fields. Variations in DVR algorithms often involve non-linear processes which make it difficult to quantify the resulting differences and also difficult to develop objective comparison metrics and methodologies. There has been research to classify image level errors generated by DVR methods such as Gaddipatti et al. [5], Sahasrabudhe et al. [23] and Williams and Uselton [31]. However, most image level metrics have limited capabilities because they analyze quantized image values only. In our earlier work [8, 9], we proposed data level metrics and a methodology to perform an in-depth comparison study using the intermediate rendering information generated by DVR algorithms. Intermediate rendering information, such as the distance a ray penetrated and the number of cells visited provides quantitative measurements that provide insight as to what data contributed to each pixel. This information is used for comparing DVR algorithms.

In this paper, we present algorithm specifications and parameters, two test data sets: **3DCheckerBoard** and **Ramp**, and image and data level metrics to be used for in-depth comparison studies of DVR algorithms. The algorithm specifications include those that are often ambiguous or unspecified in published work, but can produce considerable differences in the final rendered images. Examples include differences among interpolation and gradient calculations, pipeline order, and compositing technique. These need to be clearly identified and specified as a pre-requisite for proper comparison. This paper provides the necessary specifications for a large class of DVR algorithms. While one can see a few test data sets, such as those from the Visible Human Project (`http://www.nlm.nih.gov/research/visible/visible_human.html`), that DVR researchers commonly use, the complexity of these data sets make them less than ideal for analyzing the complex interaction of different parameters on the resulting image. This paper proposes two simple, easily reproducible data sets that help amplify differences resulting from variations in

algorithms specifications and parameter values. Finally, this paper utilizes data level metrics to enhance the comparative power of image level metrics alone, and demonstrate their usage with a number of case studies. We limit our case studies to static, regular or rectilinear, scalar volume data only.

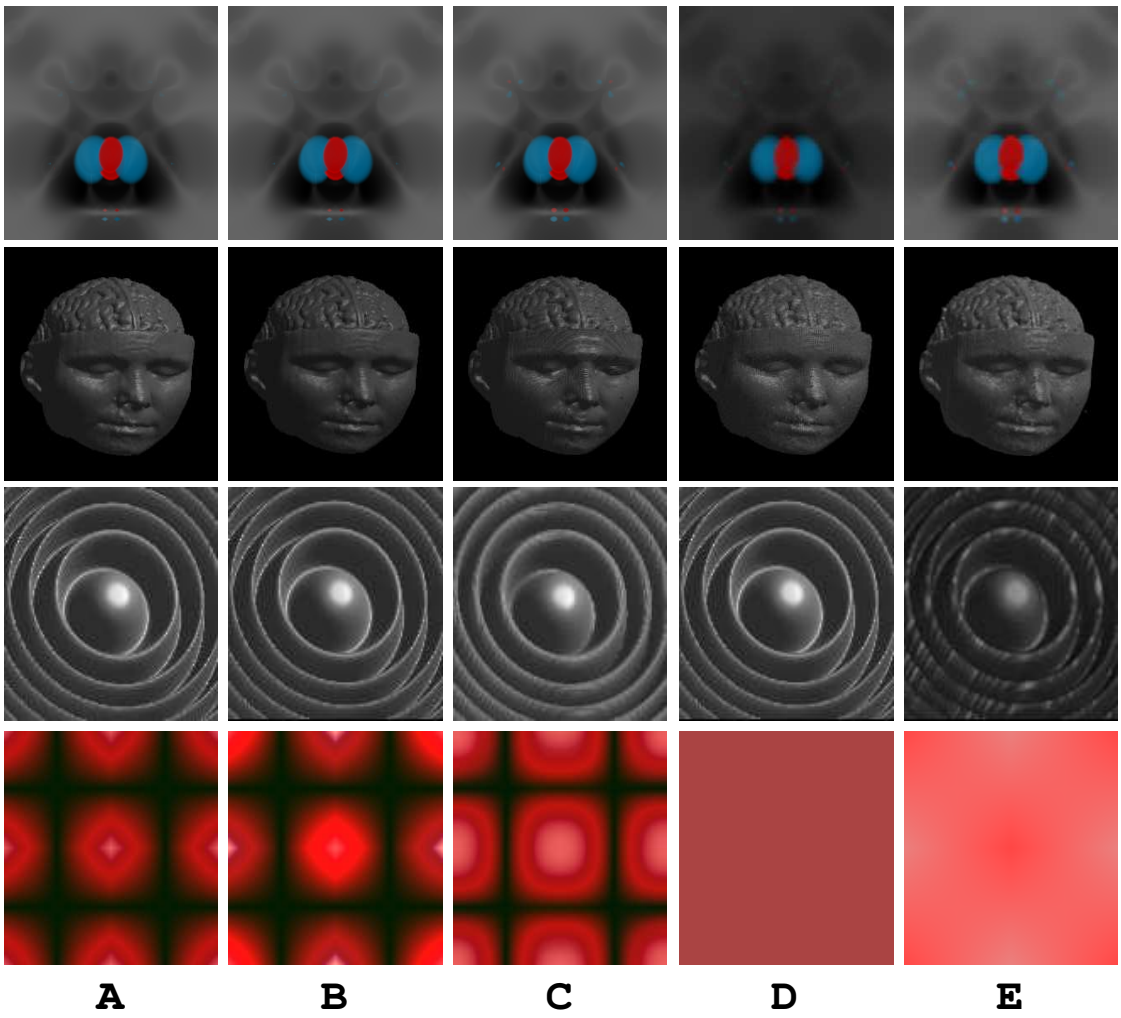

Figure 1: The volume rendered images of **High Potential Iron Protein** (top row), **University of North Carolina Chapel Hill MRI brain data** (second row), the **Marschner and Lobb**'s analytical data (third row), and our test data **CheckerBoard** (bottom row). Column D is generated by a projection algorithm while the others are generated by different raycasting variations. Details on the rendering specifications are given in Table 6.

Figure 1 graphically illustrates our motivation and direction. The first three rows show typical side-by-side image level comparison of DVR renderings of test data. Some qualitative differences can be observed but not much else beyond that. On the other hand, the bottom row of images

show DVR renderings using one of our test data sets. The qualitative differences are much more obvious. And because the structure of the data is understood, one can get a better idea of what the algorithm is doing. Later in the paper, we illustrate how quantitative measures can be obtained using data level metrics that allow one to get a deeper understanding of the effects of different algorithm specifications and rendering parameters. The new datasets and metrics highlight differences between algorithms. In real datasets there will be subtle differences, but it will be hard to say what is superior. These tools make it clear why the differences exist. It is up to the developer to determine the appropriate trade-offs for their applications and datasets.

For the rest of this paper, we discuss: relevant previous work and an overview of the comparison process; a list of rendering parameters and specifications with an example taxonomy of DVR algorithms; test data sets; comparison metrics; results on three different comparisons; and conclusions.

2 Previous Work

The importance of comparing DVR algorithms has long been recognized, but efforts are few and far in between. Previous work in comparing the quality of DVR algorithms can be grouped into four general approaches. The first approach compares two or more DVR images using a barrage of image based metrics such as those used by Neumann [20] and Wittenbrink and Somani [33]. However, one must be aware of the limitations in popular summary image statistics such as mean square errors (MSE) and root mean square error (RMSE) as pointed out by Williams and Uselton [31]. For example, these measures cannot distinguish between noise in image versus structural differences in image. On the other hand, spatial structure based metrics such as those proposed by Sahasrabudhe et al. [23], measure and highlight the extent of the inherent structures in the difference between images. Similarly, the wavelet based perceptual metrics proposed earlier by Gaddipatti et al. [5] take into account the frequency response of the human visual system on saliency measurements between two images to help steer further image generation. While these metrics may aid in the

analyses of data sets using a particular volume renderer, they are not designed to bring out the differences caused by variations in different volume renderers or different algorithm settings.

The second approach compares raw data and intermediate information gathered during the rendering process. Since this approach uses more information than the image level approach, it can provide additional comparative information, and can potentially identify reasons behind differences in DVR images. Aside from comparing DVR algorithms [8, 9], data level comparison has also been used for scalar data sets by Sahasrabudhe et al. [23] and vector data sets by Pagendarm and Post [21]. While this approach is promising, it also has a limitation. It may not be possible to use such an approach directly for some problems. For example, with DVR comparisons, a common base algorithm is necessary for collecting common comparison metrics [8, 9].

The third approach uses analytical methods to calculate the error bounds of an algorithm. Representative work in this area includes analysis of errors in gradient calculations by Bentum et al. [2], analysis of normal estimation schemes by Möller et al. [18], and errors in filtering and reconstruction operations [1, 14, 16, 19, 20, 28, 33]. The limitation of an error bound is the difficulty of gauging the actual effects directly on a visualization.

The fourth approach compares renderers by using test data to highlight differences. For example, researchers have used points and lines [20], cones and pyramids with slots [24, 26], spheres and cubes [32, 33], analytical functions [16, 19], and tori [7]. The analytical data set introduced by Marschner and Lobb [16] has also been used in comparisons of gradient filters by Möller et al. [19]. Other examples include the CT scanned Head (University of North Carolina Chapel Hill), the Visible Human Project's data and molecular simulations data such as Hipip (High Potential Iron Protein) [11, 13, 29]. While using real world data tests nuances in the interaction of an algorithm with complex data, it makes the comparison of algorithm and parameter effects more difficult. On the other hand, having simple or analytically defined test data provides a straight forward means for computing reference solutions, and can facilitate comparisons.

3 Comparison Study Overview

The comparison architecture in Figure 2 allows us to compare DVR algorithms in two different ways. In Figure 2a, either the algorithm or relevant parts of the rendering parameters (described in Section 4) are held constant to study the effects of the free variable. For example, effects of different DVR implementations can be compared by running them on the same input data and the same set of rendering parameters. The resulting images are then compared using image level comparison techniques. This is the more traditional approach for comparing DVR images and algorithms. Some obvious limitations of this approach are that comparisons are performed on quantized image values rather than higher precision intermediate data values. Furthermore, the process by which those image values are arrived at are totally ignored in image based comparison. Hence, we complement image based comparisons with data level comparisons by comparing intermediate data.

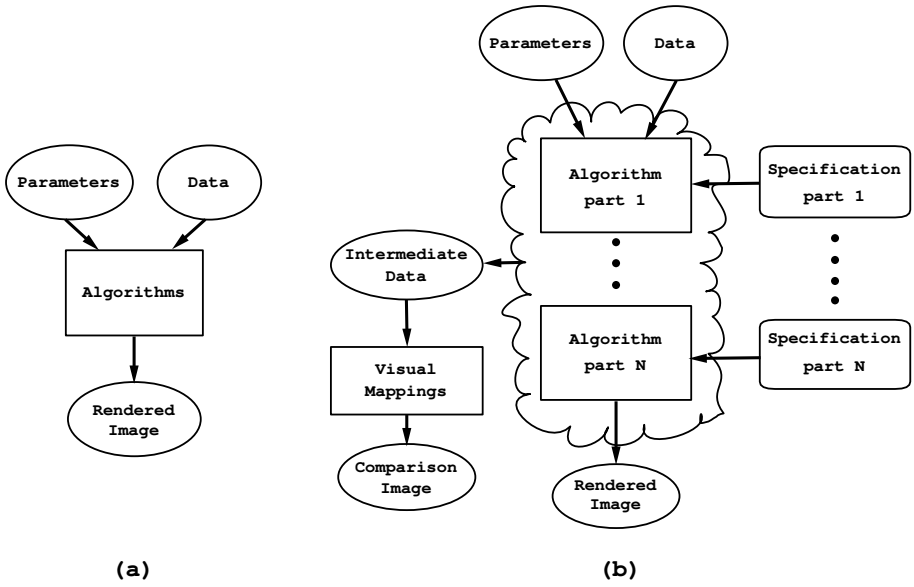

Figure 2: Overview of comparison strategies for DVR images and algorithms.

Figure 2b shows our proposed approach for comparing DVR images and algorithms. The hard-coded DVR algorithm implementation in Figure 2a is replaced with a generalized DVR algorithm implementation, described in [8, 9]. Different DVR algorithms are simulated by selection of different algorithm specifications (described in Section 4). The main advantage of this approach is as DVR algorithms are emulated their intermediate data are available. This allows one to quickly

explore DVR algorithms variations through data level comparisons.

Details of how the generalized DVR algorithm in Figure 2b is implemented can be found in [8, 9]. Essentially, because there is a large variation in different DVR implementations, a base or reference approach is first selected. The base algorithm may either be projection based or ray based. For example, Van Gelder and Kim's [25] 3D volume texture algorithm can be simulated using a raycasting base algorithm. 3D volume texture algorithm takes parallel slices of equal thickness from the volume and composites them into the final image. This can be simulated with regularly sampled rays starting with the first slice [9]. Instead of a raycasting base algorithm, a projection based algorithm can also be used to simulate other DVR algorithms [8]. The key component is a software volume scan conversion procedure used originally in Wilhelms and Van Gelder's [29] coherent projection. It scan converts the depth information behind each projected polygon. Interpolated data and color samples used in raycasting can be accounted for by integrating the values at each scan converting step. Once a base algorithm is selected, the algorithms to be compared are then faithfully simulated using the base algorithm. Intermediate information such as number of samples, distance traveled into the volume, accumulated opacities at each point along the ray are collected and compared. These can also be presented using visual mappings with standard visualization techniques such as pseudocoloring, iso-surfaces, glyphs, and textures. In this way, we can evaluate the differences in algorithms systematically and categorically using both image and data level comparison techniques.

4 Rendering Parameters and DVR Algorithm Specifications

Rigorous parameter and algorithm specifications are pre-requisites for comparison studies of volume rendered images. In Williams and Uselton's work [31], they recognized the importance of this issue and gave a listing of rendering parameters that need to be specified in order to generate volume rendered images amenable for comparison. However, they did not include the algorithm specifications which they referred to as *implementation details* of a volume rendering system. In

this paper, we make explicit distinctions between these two groups and refer to them as *rendering parameters* and *algorithm specifications*.

4.1 Rendering Parameters

Rendering parameters specify the settings that are used for a DVR algorithm to generate an image. Williams and Uselton [31] gave an extensive list which included: (a) scene descriptions, (b) viewing parameters, (c) optical model, and (d) image specification. Some details of this list include dimensions of the data set, derived and embedded objects in the data, and locations and directions of light sources. Table 1 summarizes the different parameter groups. Excluded from this list are data models and transfer functions which we consider to be more closely tied to the algorithm specification rather than the rendering parameters.

Parameter Group	Details
Scene Description	Data Set (data field names, data values and precision) Background (background color and/or texture map) Lighting (intensity, location and directions of lights) Derived and Embedded Objects (surface or procedural descriptions and their material properties and shading model)
Viewing Parameters	projection type, eye and look-at position, viewing definitions
Optical Model	theoretical optical model or light intensity differential equations, definitions of optical properties of volume density
Image Specification	image size, resolution, and format

Table 1: Parameter list for rendering environments from Williams and Uselton [31].

4.2 DVR Algorithm Specifications

DVR algorithm specifications define in detail a DVR algorithm. We classify DVR algorithm specifications into five major groups as shown in Table 2. This table illustrates the large degree of

variability of DVR algorithms. However, it is not comprehensive and does not cover frequency domain algorithms such as Malzbender's [15] Fourier volume rendering. In this paper, we limit our approach to spatial domain DVR algorithms.

Specification Group	Details
Reconstruction	geometry type (regular,curvilinear,unstructured), data location, intra-cell interpolation or approximation functions (trilinear, cubic B-spline etc.) multi-resolution parameters, sampling, footprint profiles
Classification	transfer function, surface classification functions (binary, iso-value, region boundary [13]) and any relation between transfer function and separate surface classification functions
Gradient	direct or intermediate calculation, higher order function for gradient calculation, boundary condition
Pipeline Order	order of classification of data and color samples or opacity weighting [32]
Color and Lighting	color integration method, compositing equation, choice of sample colors to be integrated and composited, lighting model

Table 2: Specification groups for DVR Algorithms.

1. Reconstruction. The reconstruction group represents the choice of algorithms for resampling discrete input data. The reconstruction process differs between image order and object order algorithms. For ray casting the reconstruction kernel and sampling pattern are specified, while for splatting the profile and weights of the splats are specified.

Specifications about how data are stored and handled are included in the reconstruction group because these affect the reconstruction process. The list includes geometry type, data locations, and intra-cell interpolation (or approximation) functions. There are four general types of data geometries: *regular* (R), *rectilinear* (RL), *curvilinear* (CL), or *unstructured mesh* (U). In this paper, we focus only on comparing *regular* or *rectilinear* grids. Data locations can be modeled as a *cell (CELL)* or *voxel (VOXEL)*. In a cell model, 8 data locations can affect material presence within

a cell and the data values are interpolated at intra-cell locations. *Trilinear* (TL) interpolation is typically used for intra-cell interpolation but some higher order functions are also used. In a voxel model, materials are centered around data locations. Various types of distance functions are used to calculate the influence (or footprints for object order algorithms) of a voxel. In this paper, we use the smoothness (or continuity) and the order of the error function (EF) to specify the higher order reconstruction functions as in Möller et al. [19]. For example, we can use a cubic function that is C^2 continuous and has an EF order of 2 for intra-cell interpolations.

Sampling pattern refers to any description regarding the distributions of sampled points in the z direction of the viewing coordinate system. There are three basic types: *regular sampling* (REG), *cell face sampling* (CF), and *volume slicing* (VS). Together with the sampling pattern, the threshold condition for terminating the rays should also be specified.

Projection based algorithms such as coherent projection and splatting use either cell projections (CELL PROJECTION) or Gaussian (GAUSSIAN) footprints to composite material contributions from a cell (or voxel) to the screen. A set of polygons are often used to approximate the influence from a voxel (or cell). The profiles of the set of polygons should be specified along with any approximation functions used for the material accumulations.

2. Classification. The classification group refers to mapping methods that map data values to different materials or surfaces. It includes transfer functions, and surface classification functions. The data values are typically mapped to color (red, green, blue) and opacity values. A subtle distinction should be made in how the colors in the classification functions are defined. In *associative* (AS) classification (or transfer) functions, a user defines RGB values to be influenced by opacity values. The intensities of RGB components are dependent on the opacity function defined, which seems to be the majority of the cases. In *non-associative* (NAS) functions, intensities of RGB components are independent of opacity values. In other words, NAS or AS specifies whether the transfer function for color and opacity channel have the same scalar domain or not. Users should define RGB intensities as material properties and opacity acts only as an occlusion factor at the

sample points. However, the opacity components affect the RGB intensities of samples when the color is integrated over a distance. This is also related to color integration and compositing equation specifications. Some published work does not make a clear distinction in this category. We will clear some of these up using a taxonomy of algorithms later in this section. Most algorithms use one of three volume surface classifications: *Binary*, *Iso-value Contour Surface* or Levoy's [13] *Region Boundary Surface* classifications. In *Binary* classification, a surface is defined if the data value falls within a specified range. For *Iso-value Contour* and *Region Boundary* surfaces, a surface is defined as a function of data value and its gradient. In *Iso-value Contour*, a fuzzy surface is created around a single iso-value. On the other hand, in *Region Boundary*, transitions among multiple surfaces can be defined.

3. Gradient. The gradient group represents the choice of algorithms for computing normals from the volumetric data that are used to improve the shading and appearance of material. The most popular method of calculating gradients uses the *Central Difference Operator* (CENTDIFF) as in Levoy [13]. This operator computes gradients at data locations using differences between neighboring data values in x, y, z direction. Its one-dimensional convolution kernel is

$$D_{x,y,z} = [-1 \;\; 0 \;\; 1] \tag{1}$$

The gradient vectors for locations other than at data locations are interpolated using the gradients at the eight nearest surrounding data locations. Another method is to compute gradient vectors situated between data locations using differences in data values at the immediate neighbors. This is called the *Intermediate Difference Operator* (InterDiff) [26].

$$D_{x,y,z} = [-1 \;\; 1] \tag{2}$$

The differences in locations of gradient vectors calculated, using these operators, are illustrated in Figure 3 (in 1 dimension, for convenience).

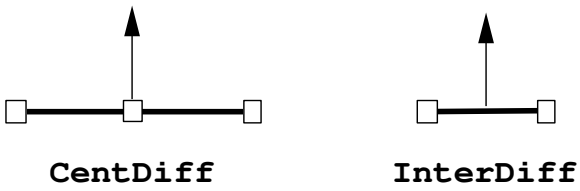

Figure 3: Locations of the gradients calculated in Central Difference Operator (CentDiff) and Intermediate Difference Operator (InterDiff). Data locations are shown with squares while arrows are the gradients.

More expensive variations involve using more neighboring data locations and correspondingly higher order filters. In this paper, we specify the filters by using the smoothness (or continuity) C and error function (EF) order as described in Möller [19]. They are used in the same way that reconstruction functions are specified in the data model group. We also need to specify how to evaluate gradient vectors at the boundary of the volume data as there may be ambiguities there. For example, volume data may be padded with null values outside the border or they may be padded with their immediate neighbor's values.

4. Rendering Pipeline Order. The pipeline order group defines the sequence of material classification and interpolation. We identify three variations in this paper, and refer to them as *data interpolation* (DATA), *color interpolation* (COLOR) and *color interpolation with opacity weighting* (COLOR-OW). First, at arbitrary sampling locations, one can interpolate and then classify data values (DATA). Second, in algorithms such as Levoy's [13], the data are classified at the voxel locations and colors are interpolated at the sample locations (COLOR). The third way is to classify the material at voxel locations and then interpolate colors with opacity-weighting at sample points as in Wittenbrink et al. [32]. The detailed comparisons of these three approaches, in terms of material classification, rendering qualities, and computational complexities, are described in Wittenbrink et al. [32].

5. Color and Lighting. The color and lighting group relates to the illumination, shading, and compositing process. Raycasting using regular sampling may be used with a *discrete* (DISC) compositing process wherein the sampled color is directly used without additional consideration to the

sampling distances. However, when samples are taken at non-regular distances (such as CF sampling), the inter-sample distances are considered and *integrated* (INTEG) along the path between sample colors. In some algorithms, a *constant* (CONST) is multiplied to adjust the color intensities. One way to visualize sampled volume data is to use a simple method such as the maximum intensity projection (MIP). However, in most of DVR algorithms, sample colors are composited. When the color is composited in *back-to-front* (BF) or *front-to-back* (FB) order, different DVR algorithms choose either a *single color* (SINGLE) of the current sample point or an *average of two colors* (AVERAGING) to represent the sampling interval. The latter choice tends to result in smoother images. Sampled colors can be composited using *associated* (AS) (Equation 3) or *non-associated* (NAS) (Equation 4) color compositing equations (comp eq). Different compositing approaches can be shown to be the result of different particle models such as Max's [17] absorption plus emission and emission only [17, 29]. For a given sampled (and integrated) color (C), different algorithms use one of following equations

$$\tilde{C}_{new} = (1 - \alpha_{front})\tilde{C}_{back} + \tilde{C}_{front} \tag{3}$$

$$\tilde{C}_{new} = (1 - \alpha_{front})C_{back}\alpha_{back} + \tilde{C}_{front} \tag{4}$$

Here $\tilde{C}$ $(= \alpha C)$ is an associated color (opacity-weighted) , α is the opacity, and C is an unassociated (unweighted) color. Equation 3 is used for back-to-front or front-to-back while Equation 4 is for front-to-back evaluation. The NAS equation often assumes that the sampled color is not associated with opacity yet. Algorithms with the AS equation either treat the sampled color as associated color or perform some calculations that consider opacity values. A general description of the lighting model should be given such as Phong.

4.3 Detailed Algorithm Specifications

The algorithm specifications described in the previous section cover the major sources of differences in DVR algorithms. More precise specifications need to be made if an exact comparison is

desired. However, it may not be always possible to achieve this. For example, when volume cells are projected, the projected polygons are likely to be rendered in hardware. Rendering results vary depending on the hardware scan conversions where detailed specifications are often hard to obtain. Fortunately, software simulations of the scan conversion process can standardize such hardware dependencies and bound the discrepancies to within a certain range. For example, we simulated the coherent projection algorithm and measured the differences between color values in all the vertices of all the projected polygons with the original algorithm [8]. The differences were less than 10^{-7} in the scale of 0.0 to 1.0 for each color channel (in multiple viewing directions) effectively machine epsilon for a single precision floating point value. Another example of detailed algorithm specification would be the precision of color compositing. A lower precision of the opacity channel can produce dramatically different rendering results. It is important to make efforts to have a complete specification of all the rendering parameters and algorithm specifications.

4.4 Taxonomy

algorithm	data location	pipeline order	sampling	tr fn	footprint
Levoy [13]	CELL	COLOR	REG	NAS	
Coherent Proj. [29]	CELL, VOXEL	DATA	CF	NAS	CELL
Splatting [12, 27]	VOXEL	DATA		AS	GAUSSIAN
Shear-warp [11]	CELL	COLOR	CF	NAS	
Voltx [25]	CELL, VOXEL	COLOR	VS	NAS	
Opacity-Weighting [32]	CELL, VOXEL	COLOR-OW	R	AS	

Table 3: Some algorithms with specifications in data location (CELL or VOXEL model), pipeline order (COLOR, DATA, or color interpolation with opacity-weighting (COLOR-OW)), sampling (Regular (R), Cell face intersection (CF) or Volume slicing (VS)), transfer function (tr fn) (Associative (AS) or Non-Associative (NAS)) and footprint profile (footprint) (Cell projection (CELL) or Gaussian (Gaussian)).

Here, we give a taxonomy of some popular DVR algorithms based on their specifications. This taxonomy can be used as a guide to study the algorithms and explains specifications that are easily neglected and ambiguous in some published work. Table 3 and Table 4 show specifications of some algorithms. Algorithms such as ray casting and coherent projection [13, 29] can be used more

algorithm	surf. class.	color integ.	direction	comp. color	comp eq
Levoy [13]	ISO,RB	DISC	FB	SINGLE	NAS
Coherent Proj. [29]		INTEG	BF (FB)	AVERAGING	AS
Splatting [12, 27]		INTEG	FB	SINGLE	AS
Shear-warp [11]	RB	INTEG	FB	SINGLE	NAS
Voltx [25]	BIN	INTEG	FB (BF)	AVERAGING	AS
Opacity-Weighting [32]	BIN	DISC	FB (BF)	SINGLE	AS

Table 4: Algorithms (as in Table 3) with specifications in classifications (Region Boundary Surface (RB), Iso-value surface (ISO) or Binary (BIN)), color and lighting groups that include whether the color integration is used (INTEG) or not (discrete compositing (DISC)), compositing direction (front-to-back (FB) or back-to-front (BF)), compositing color (single sample color or averages of two sample colors), and compositing equation (associative (AS) or non-associative (NAS)).

sampling pattern	*color compositing*			
	Single Color		*Averaging*	
	NAS eq	AS eq	NAS eq	AS eq
regular (R)	Levoy[13]	Opacity-Weighting[32]		
cell face (CF)	Shear-warp[11]			

footprint profile	*color compositing*			
	Single Color		*Averaging*	
	NAS eq	AS eq	NAS eq	AS eq
cell projection				Coherent Proj.[29]
gaussian		Splatting[12, 27]		

Table 5: Taxonomy tables of DVR algorithms using sampling pattern, footprint profile, compositing color and equation (Non-Associative (NAS) or Associative (AS)). Image order algorithms are classified by their sampling patterns, while object order algorithms are classified by their footprint profile.

generally but the specifications show the typical usage of the algorithms as published. However, algorithms such as *shear-warp* [11] and *voltx* [25], have performance advantages when used with the specific settings, so comparisons with other settings might degrade performance considerably. The list of algorithms in both tables are not meant to be exhaustive but demonstrate how some published algorithms may be specified with our list of specifications. Table 5 shows an example of an algorithm classification in terms of sampling/projection profile and color compositing groups. The blank entries are combinations that we have not reviewed or do not have published results for.

5 Test Data Sets

We used the goals of simplicity, generality, and maximizing rendering differences to define two test datasets: **3DCheckerBoard** and **Ramp**. The **3DCheckerBoard** is defined as voxel values,

$$V[i,j,k] = \begin{cases} L & \text{if } (i+j+k)/d \text{ is odd} \\ H & \text{otherwise} \end{cases} \tag{5}$$

Here the voxels i,j,k over the domain $[0 \ldots n-1]$, and take values of L (low) or H (high). Distance, d, is an integer constant that allows the checks to be $d = 1, 2, 3, \ldots$ in width in each dimension. The datasets are defined to be $n \times n \times n$ in size. Figure 4a shows an example of a **3DCheckerBoard** dataset. The **Ramp** is defined as voxel values,

$$V[i,j,k] = L * (1 - \beta[d]) + H * \beta[d] \tag{6}$$

$$\beta[d] = d \,/\, (n-1), \qquad where\ d = i,\ j,\ or\ k \tag{7}$$

Voxel i, j, k varies linearly from L (low) to H (high) as $i,\ j$, or k increase from $0 \ \ldots \ n-1$. The Ramp can vary in any of the three directions individually or simultaneously by using a different $\beta[\,]$. Figure 4b shows an example Ramp dataset. For simplicity we do not discuss pre-filtering the datasets.

6 Metrics

Although some new image level metrics have been developed to quantify structural and perceptual differences [5, 23, 31], we use two basic image level metrics namely: MAE (Mean Absolute Error) and RMSE (Root Mean Square Error). While it has limitations or can be misleading as pointed out by Williams and Uselton [31], RMSE is one of the most widely used image level metrics. We use

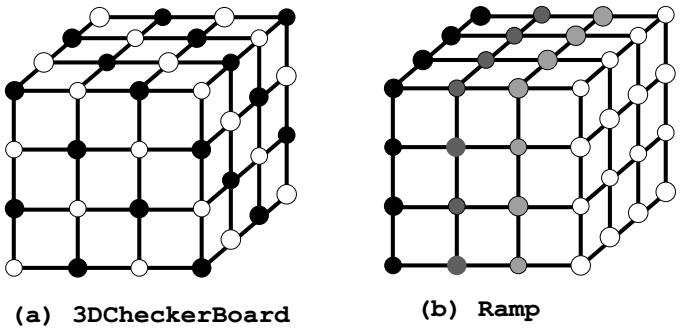

Figure 4: Test data example shown in cell model; (a) **3DCheckerBoard** ($n = 4, d = 1$). The black and white sphere show the high (H) and low (L) value. (b) Ramp ($n = 4$). The data values changes from the maximum (black) to the minimum (white). The interior data points are omitted to reduce clutter in these illustrations.

MAE as an additional image metric. These are defined below:

$$\begin{aligned} RMSE &= \sqrt{\sum_{i,j}[\mathbf{A}(i,j) - \mathbf{B}(i,j)]^2/N^2} \\ MAE &= \sum_{i,j}|\mathbf{A}(i,j) - \mathbf{B}(i,j)|/N^2 \end{aligned}$$

where **A** and **B** are images (of size $N \times N$) to be compared.

We include these image level summary statistics for measuring general differences as a point of reference and because they are well known. Perceptual image metrics are not included because the test data sets are already supposed to highlight differences in the algorithms. In fact, one can easily observe structural patterns in the images in the next section. Perceptual metrics would simply produce high values for such images with obvious spatial structures. Hence, the primary metrics that we use in Section 7 are data level metrics. Several types of data level metrics that utilize intermediate data were introduced in [8, 9]. Recall that in order to collect data level metrics that can be compared across different classes of DVR algorithms, the algorithms to be compared must first be simulated by a common base algorithm. This step also ensures that the intermediate rendering data are registered and ready for comparison.

In this paper, we use several *threshold based metrics* such as NS (Number of Samples), NSD

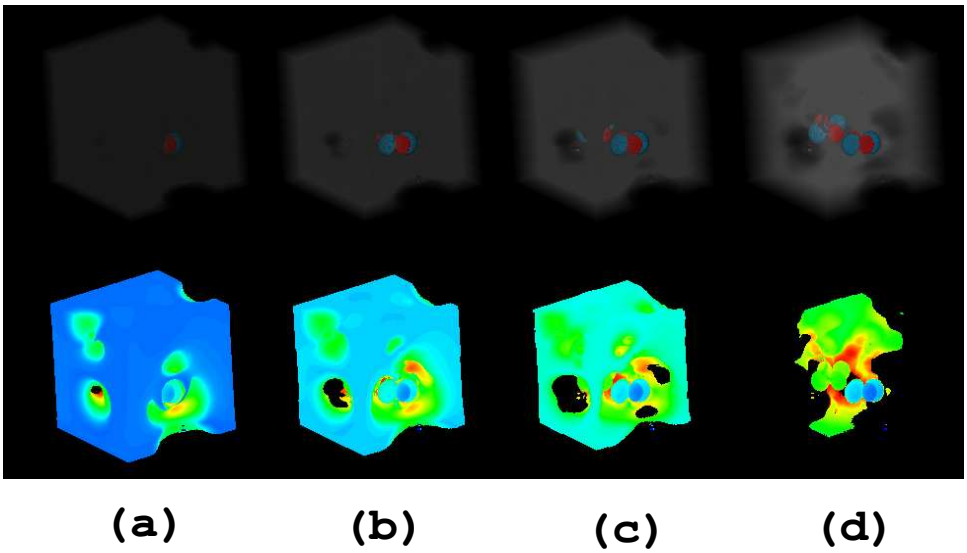

Figure 5: DVR images (top row) with corresponding visualizations for the number of samples (NS) metric (bottom row). NS is accumulated until the given opacity threshold is reached for each pixel at (a) 0.10, (b) 0.15, (c) 0.20, and (d) 0.30. Regular ray sampling is used to render this Hipip data set. Black regions indicate that rays entered and exited the volume without reaching the opacity threshold.

(Number of Samples Differences) which measure the difference in the number of samples, and Corr (Correlation of sampled colors) which measures how well correlated are the values used in arriving at a pixel color. These metrics are called threshold based because they are collected as long as a specified threshold has not been reached. For example, NS counts the number of values contributing to a pixel color while the ray has not reached an opacity threshold.

Figure 5 compares the number of sample metric on the Hipip data set with four different opacity thresholds. A rainbow color map is used for each threshold to show fewer samples (blue) to many samples (red).

To calculate the correlation between two vectors of sample colors collected by two different algorithms, we let V and W be two random variables representing the two normalized sample color vectors along the viewing direction. The statistical correlation ρ between these two random variables is defined by

$$\rho(\vec{V},\vec{W}) = \frac{cov(\vec{V},\vec{W})}{\sigma_V \sigma_W} = \frac{E[(\vec{V}-\mu_V)(\vec{W}-\mu_W)]}{\sigma_V \sigma_W} \tag{8}$$

where $cov(V, W)$ is the covariance of the two random variables, μ_V and μ_W are the means of of $\vec{V}$ and $\vec{W}$, E is the expectation, and σ denotes standard deviation of the random variable. The closer ρ is to 1, the more correlated the two sample color vectors are. The correlation metric (Corr) at each pixel location may be color mapped (as in Figure 14) or averaged to obtain a mean correlation value for the entire image (as in Table 9).

Sample colors are usually represented by separate red, green, and blue color and opacity channels which may or may not be correlated to each other. Hence, the correlation metric is calculated for three color channels to provide additional information when comparing two different renderings.

7 Results

In this section, we present three examples to show how our test data are used in comparison studies of DVR algorithms using both image and data level metrics. In most of the examples, parallel projections with simple orthographic views are used. The simple viewing setup coupled with data sets that are easy to understand helps us in understanding and pinpointing the effects of different algorithm specifications as discussed in the examples below. That is, the simple viewing setup produces patterns in the resulting image that can be readily explained given the algorithm specifications. On the other hand, changing the projection from parallel to perspective (see Figure 9) or changing to a non-orthogonal view (see Figure 10) may be less effective for this task. Another reason why we do not recommend using perspective projection is because some algorithms, such as coherent projection, are limited to parallel projections.

When looking at the images in the three examples to follow, the rendered images may appear to be abstract and not what one might think the data ought to look like. It is because rendering results of our test data sets can vary widely depending on algorithms and their settings. This is in fact one of the main reasons for designing test data that are very simple. They immediately bring these differences to the forefront and raise our attention, whereas more complex data set renderings

would not be easy to interpret. Furthermore, because we know the simple structure of the data sets, the appearance of the renderings directly helps us explain the effects of the different algorithm specifications. This is achieved with the aid of data level metrics as described in the examples below. Of course, as can be seen in the images in this section, some of the differences are more significant than others. The ability to alter one or more algorithm specification at a time, allows us to determine which combinations have more impact on the resulting images.

7.1 Pipeline Order, Compositing, Data Model

In this example, we experimented with variations in specification groups such as data model, rendering pipeline order, and color integration. Variations in algorithm specifications are given in Table 6. Other specifications such as sampling patterns are held constant and their details are described in the Appendix (Figure 17). Figure 6 shows the rendered images of **3DCheckerBoard** with different algorithm variations (A to E) and their corresponding difference images (F to I). The difference images use image A as the reference image to be compared. The data set used is a 3^3 **3DCheckerBoard**. The transfer function and the actual data are described in the Appendix. The volume data is rendered with a cell model.

image	algorithm	data model	pipeline order	color integ	comp color
A	raycasting	tri-linear	DATA	INTEG	AVERAGING
B	raycasting	tri-linear	DATA	INTEG	SINGLE
C	raycasting	cubic filter	DATA	INTEG	AVERAGING
D	Coherent Proj. [29]	tri-linear	DATA	INTEG	AVERAGING
E	Levoy [13]	tri-linear	COLOR	DISCRETE	SINGLE

Table 6: Specifications for the algorithms that generated images A to E in Figure 6.

An obvious difference can be noticed by simply changing the order of operations in the pipeline. For example, interpolated data values are used to index into a transfer function in images A, B, C while data values are converted to color values and then interpolated in image E. By interpolating data values first, and in combination with a transfer function, a full range of material can be extracted from this simple data set. On the other hand, by converting data to color values first, we

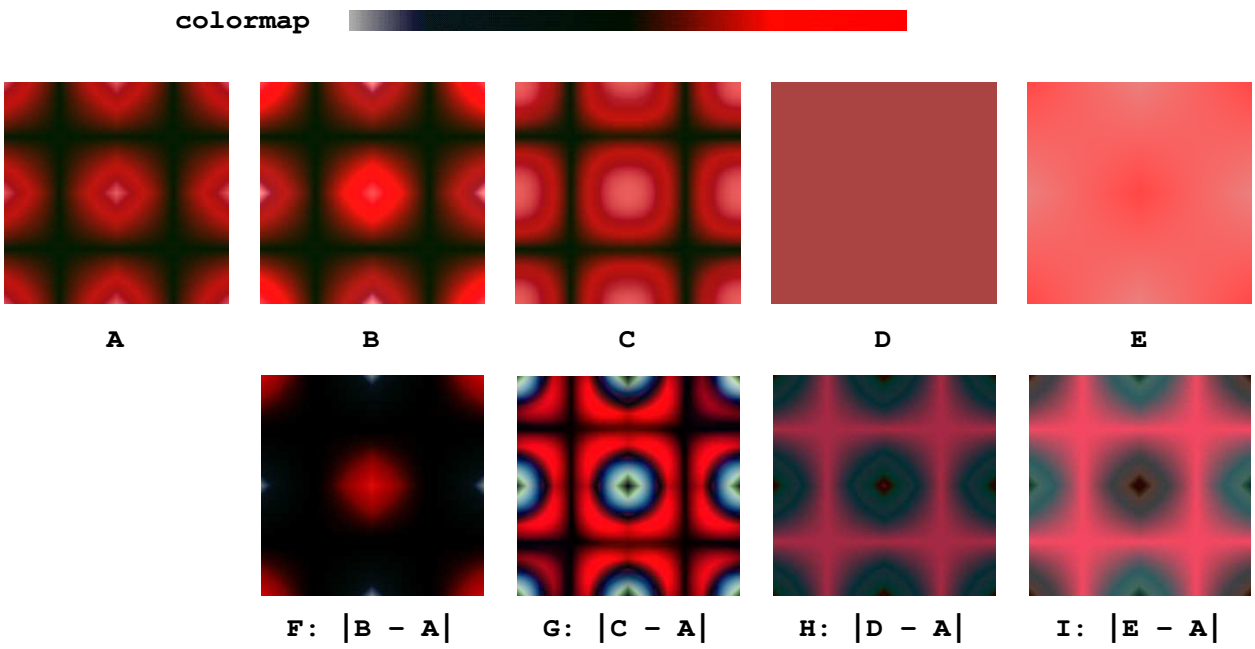

Figure 6: The volume rendered images of the 3DCheckerBoard data with different specification settings. Images A to E (Same as the bottom row of Figure 1) are generated by DVR algorithms with specifications given in Table 6. Image F to I are differences of B to E with the reference image A respectively. All images are 256×256. The color map for the transfer function is also displayed above images and its details are provided in the Appendix.

are essentially seeing the blending of only two materials – either red or white in image E. Image D, produced by Coherent Projection, appears as a homogeneous block because in this view, the volume cells are projected into four abutting square polygons where the colors at the vertices of each projected polygon are averaged between the front and back colors (materials). These colors are either red or white. Hence, the interpolated colors for each polygon are homogeneous. In addition to the difference in intensity between images D and E, some structural differences can also

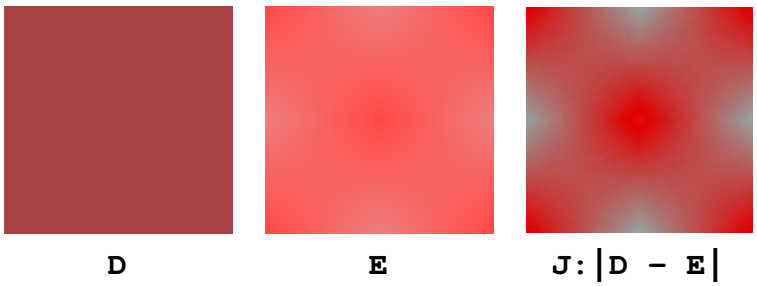

Figure 7: Image J shows difference image between images D and E of Figure 6.

be seen in their difference image as illustrated in Figure 7. This can be attributed to the fact that the algorithm for image E uses a discrete color integration and compositing with a single sampled color, while the algorithm for image D uses the averaged color of the front and back samples along the ray.

Both algorithms for images A and B use data interpolation (tri-linear) at the sample points. The difference stems from the choice of color to be composited (*comp color*). Algorithm A uses averaged values between two samples (such as front and back values) while the one for B uses a single sample value. The differences are more subtle and the resulting difference image (see image F) as well as summary statistics on the comparison also yield the least difference (see Figure 8). One can see a more noticeable difference between images A and C, where the type of interpolation function is different while the other algorithms specifications are held constant. Image C is generated with a cubic filter function while image A is generated with a tri-linear interpolation function. This results in a smoother transition of intensity from the data value to the cell boundary.

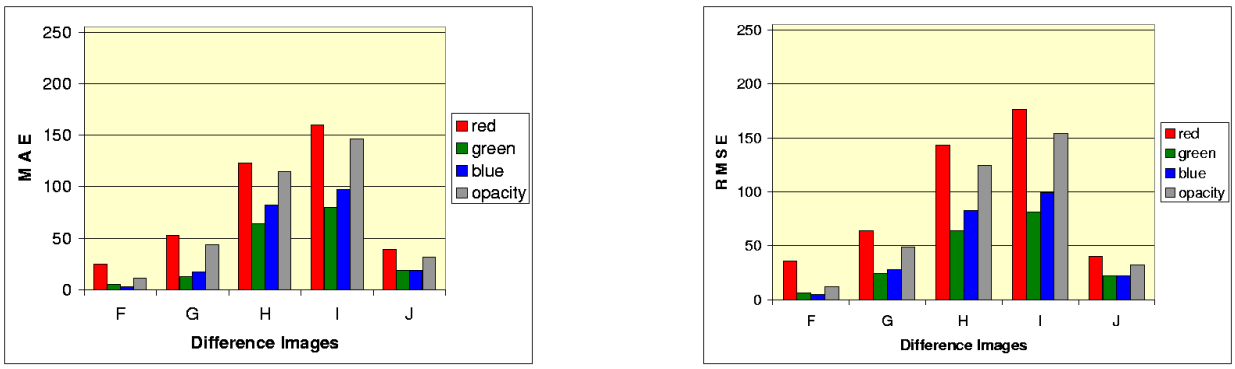

Figure 8: Mean Absolute Error (MAE) and Root Mean Square Error (RMSE) in RGBA channel for algorithm differences in **3DCheckerBoard**. F, G, H, I, and J are difference images from Figures 6 and 7.

The examples shown in Figure 6 demonstrate how the **3DCheckerBoard** can be used to identify and estimate the differences between variations in a wide range of parameters for a given transfer function. The RMSE and MAE image level measurements in Figure 8 show that we obtain the biggest difference when we vary the rendering pipeline order (I). On the other hand, changing the

choice of color compositing (F) produced the least difference.

We reiterate why it is important to use simple data sets in analyzing different algorithm variations. Figure 1 shows how our test data set compares to Marschner and Lobb's test data for the same example as Figure 6. Our test data more clearly indicates differences amongst the variations. Furthermore, it is also important to use viewing parameters that do not unduly complicate the analysis.

So far we have used a simple orthogonal view using parallel projection to clearly demonstrate the effectiveness of our test data. However, one can do a similar analysis using different settings for a more complete comparison study of algorithms. Figure 9 illustrates what happens with perspective projection, and Figure 10 compares non-orthogonal views. The differences among algorithms in Figure 9 are not as dramatic. Minimal additional information about the algorithm is gained by the perspective views, and they complicate the analysis task. In image D of Figure 10, Coherent Projection shows more material content because each volume cell is projected into more than one polygon. While additional information is made available in the images, the patterns in the resulting images are highly dependent on the viewing angle, and also complicates the analysis task.

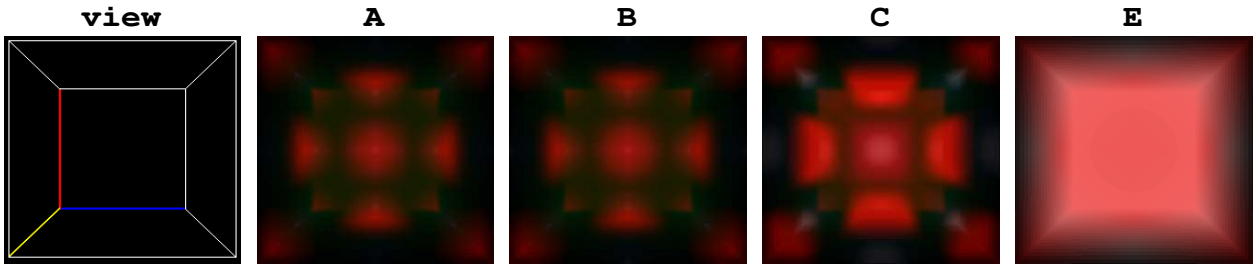

Figure 9: Renderings of algorithm A, B, C, and E using a perspective view.

7.2 Surface Classifications

In this example, we demonstrate how the **Ramp** data with $n = 4$ can be used to study variations in surface classification functions. The data has a minimum of zero and maximum of 255 and changes linearly along the x-direction (from the left to the right in the images). The detailed specifications of the surface classifications are described by Table 10 to 13 in the Appendix. We

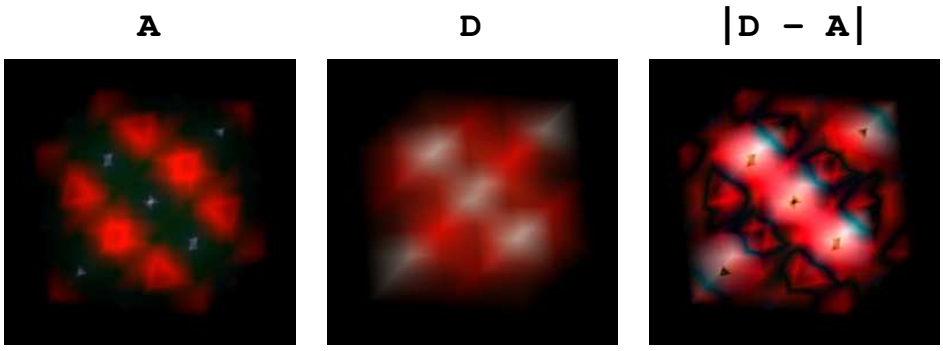

Figure 10: Renderings of algorithm A and D using a non-orthogonal viewing angle.

used a raycasting algorithm for this example. All images (256×256) are generated with identical algorithm specifications except for those specified in Table 7. Binary Surface classifications are compared with other similarly defined surface classifications. We highlight some areas of interest with rectangular boxes.

Image Index	pipe order	surf. classification
A	DATA	Binary
B	COLOR	Region Boundary
C	DATA	Binary
D	DATA	Iso-value Contour

Table 7: DVR pipeline order and surface classification methods for the images in Figure 11.

Binary classification is used in Figure 11 A. That is, any data between 127 to 255 are classified as a certain material, while data values between 0 and 126 are treated as empty space. It shows the location of the volume surface where data values are equal to or higher than 127. Figure 11 B shows the corresponding rendering using Levoy's [13] Region Boundary Surface classification. It shows a more gradual transition from the surface material to the empty material boundary. The light blue lines show the grid lines for i = 1 and i = 2. The last two visualizations on the top row show data level analyses in the transition region. Figure 11 $\mathbf{NS}_{B,\alpha=0.75}$ shows the number of samples needed to accumulate up to the opacity of 0.75 at each pixel in Fig. 11 B. The values of $\mathbf{NS}_{B,\alpha=0.75}$ are mapped to the standard rainbow color map. The black areas indicate the regions where pixels did not reach the opacity threshold. Closer to the i = 1 grid line, more samples are

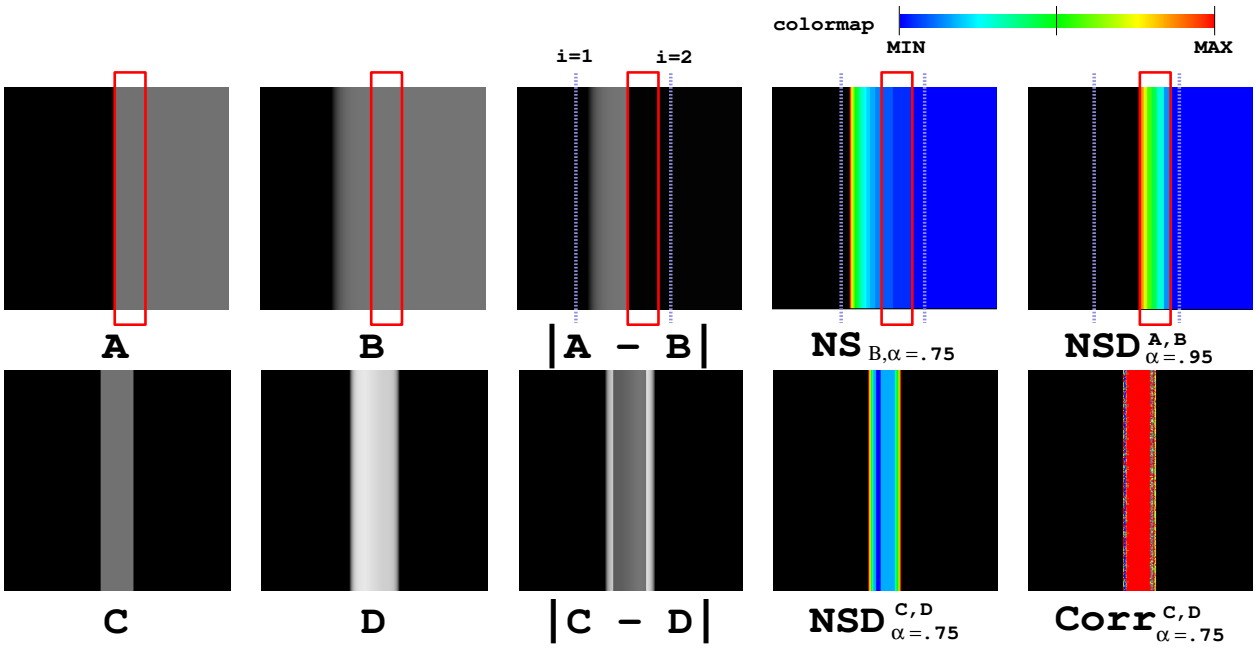

Figure 11: The volume rendered images of **Ramp** data with A : Binary classification with data interpolation, B : Region Boundary Surface classification similarly defined as A. C : Binary classification with data interpolation, D : Iso-value Contour Surface classification similarly defined as C. The color map used to visualize metrics is shown on top.

needed to reach the accumulated opacity 0.75. In contrast, Binary classification (A) requires a uniform **NS** value for half of all the pixels in the image, where there is surface material.

The rightmost image on the top row of Figure 11, $\mathbf{NSD}^{A,B}_{\alpha=0.95}$, shows the difference in the number samples needed to reach the threshold $\alpha = 0.95$ for each pixel in Figures 11 A and 11 B. The metric is collected only if both algorithms A and B reach the threshold (0.95) opacity for that pixel. Otherwise, the pixel is colored black. Although the image level metric ($|A - B|$) does not show considerable differences in the highlighted region, it confirms that there are differences in the number of samples needed to reach the same opacity, in this case, $\alpha = 0.95$. Using data level metrics such as these, a user can examine how algorithms differ in different regions of the volume data. Table 9 gives some additional metrics such as $\mathbf{NSD}^{A,B}_{\alpha=0.75}$ and sample color correlations at each pixel that are averaged over all non-black pixels.

The bottom row of Figure 11 shows differences between a Binary Surface classification and an Iso-value Contour Surface classification. Unlike Binary classification, the thickness of Iso-value

Contour surface can be controlled by the region transition thickness (r) and gradient magnitude around surfaces (see Table 13 in the Appendix). The differences can be measured and analyzed similar to the top row in Figure 11 using both image and data level approaches. Summary statistics of the images in Figure 11 are presented in Tables 8-9. They suggest that we generally have bigger differences in $|C - D|$ than $|A - B|$. The image level metrics (MAE, RMSE) of $|A - B|$ can be misleading because they are averaged over the larger area to be compared. The data level metrics provided more contextual explanations for the differences. For example, $MeanCorr^{A,B}_{\alpha=0.75}$ (Table 9) shows high correlation of sampled color but lower values in opacity channels. This suggests that the main source of difference was from sampled opacity values. It should be noted that these observations do not represent any general quality comparisons between surface classifications. Surface classification definitions can create large differences. This example simply demonstrates how our simple test data and metrics can be used to estimate and investigate the nominal differences in the user-specified surface classifications. Compared to data sets such as CTHead and MRBrain used in Figure 1, the simplicity of the **Ramp** data makes it superior in measuring effects of different surface classification alternatives. The data level metrics aid in finding the sources of differences and in finding the closest alternative to a given surface classification.

Image Index	% non-black pixel	MAE	RMSE
A - B	50.4	(2.99, 0.011)	(2.99, 0.036)
C - D	14.5	(105.3, 0.87)	(105.7, 1.63)

Table 8: Mean Absolute Error and Root Mean Square Error in color (grey scale) and opacity channels for algorithm differences with **Ramp** data.

Image Index	$NSD_{\alpha=0.75}$	$NSD_{\alpha=0.95}$	$MeanCorr_{\alpha=0.75}$	$MeanCorr_{\alpha=0.95}$
A - B	(0,2)	(0,7)	(0.99, 0.644)	(0.67, 0.40)
C - D	(2,8)	(12,18)	(0.77,0.30)	(0.17,0.03)

Table 9: Number of Samples Differences (**NSD**) and Mean Correlations (**MeanCorr**) at two different threshold conditions on the accumulated opacity (α) at each pixel. Statistics for NSD are given in (minimum, maximum) pairs. Statistics for MeanCorrs are given in (color, opacity) channel pairs, and are measured by averaging over all non-black pixels.

7.3 Gradient Calculations

Figure 12 demonstrates a different usage of **3DCheckerBoard** for measuring differences between gradient calculation methods. All images are rendered using the Region Boundary Surface classification with data interpolation (DATA). This volume surface classification is usually used with color interpolation as in Lacroute [11] and Levoy [13]. However, we use data interpolation instead to illustrate the differences in the gradient calculation. The viewing direction is orthogonal to a face of the volume's bounding box. The data size is 7^3. The material colors and the surface classifications are given in Figure 18 of the Appendix.

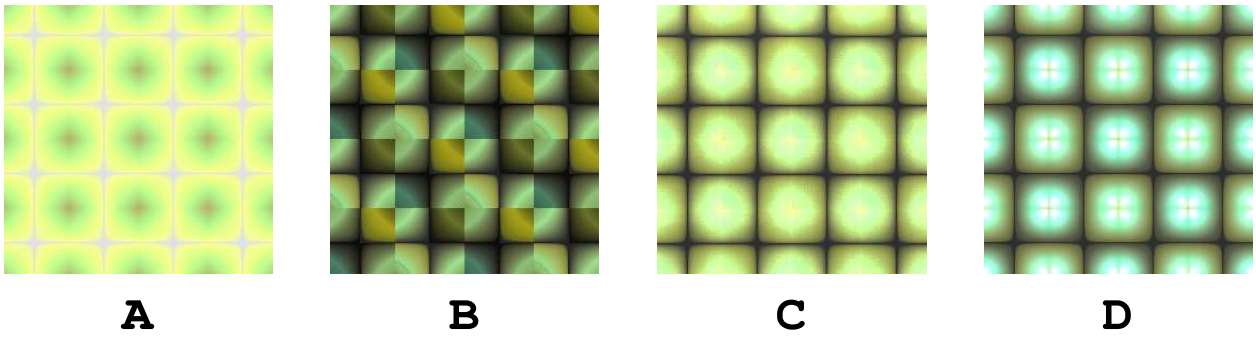

Figure 12: The volume rendered images of the 3DCheckerBoard data (n = 7) using different gradient calculation methods. (A) 6 point Central Difference Operator, (B) Intermediate Difference Operator, (C) Linear First Derivative Filter (C-0, 1EF) , (D) Cubic First Derivative Filter (C-1, 4EF). All images are 256×256.

In Figure 12A, the algorithm uses the popular 6 point Central Difference Operator (CentDiff) at the data points. The gradients are interpolated by tri-linear functions at any intra-cell sample points. In this case, the gradient magnitude will always be zero because data values alternate and hence are the same for every other point. Because of this, Figure 12A shows the rendering of ambient colors only.

Figure 13 illustrates the difference between CentDiff and InterDiff in 1D. InterDiff uses two immediate neighbors to calculate the gradient vector halfway between the two data locations. Because the data alternates between high and low values, the gradient vectors will be maximal and also alternate in direction. Figure 12B shows the effect of interpolating these alternating direction gradient vectors. Figures 12C and 12D use first derivatives to compute gradient as described in

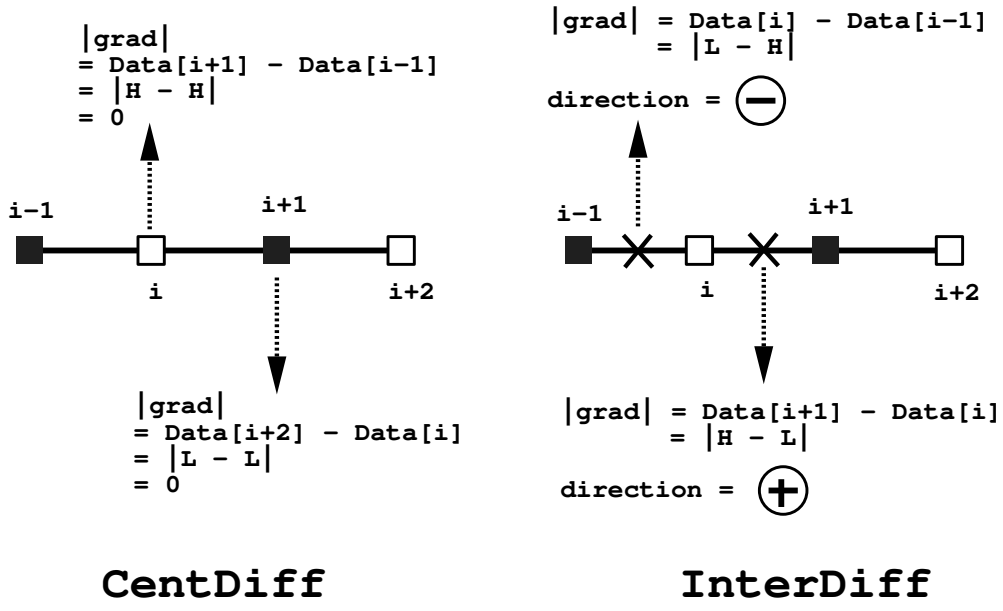

Figure 13: The difference between Central Difference Operator (CentDiff) and Intermediate Difference Operator (InterDiff) on **3DCheckerBoard** are shown in 1D. White square represents the lowest (L) and the black square the highest (H) data values in the range of $\{L, H\}$.

Möller [19]. The gradient calculation methods are Linear First Derivative Filter (C-0, 1EF) in Figure 12C, and Cubic First Derivative Filter (C-1, 4EF) in Figure 12D. Note that the grid structure shown in the images is not the grid structure of the volume. In Figure 12A, the darker and slightly reddish areas are where grid points are located because we defined such material color at the data points (Figure 18a).

Figure 14 shows the difference images of Figure 12 and visualizations of the correlations between sample colors at each pixel. The difference images show that we generally have the largest differences at the midpoints of the volume cells. $Corr^{A,B}_{\alpha=0.1}$ is the correlation of two different sample colors that have been generated by algorithm A and B along the viewing direction at each pixel of Figure 12. Corresponding sample vectors are collected along the viewing direction until both algorithms accumulate the threshold opacity 0.1 at each pixel. We can examine all the color components but, in this example, we include visualizations for the green color component only. Each difference image and data level metric shows a distinct pattern. The rendering differences of CentDiff vs InterDiff, $|A - B|$ of Figure 14, is brighter overall compared to $|A - C|$ and $|A - D|$. Generally, the regions around data points have higher correlations than other locations, although

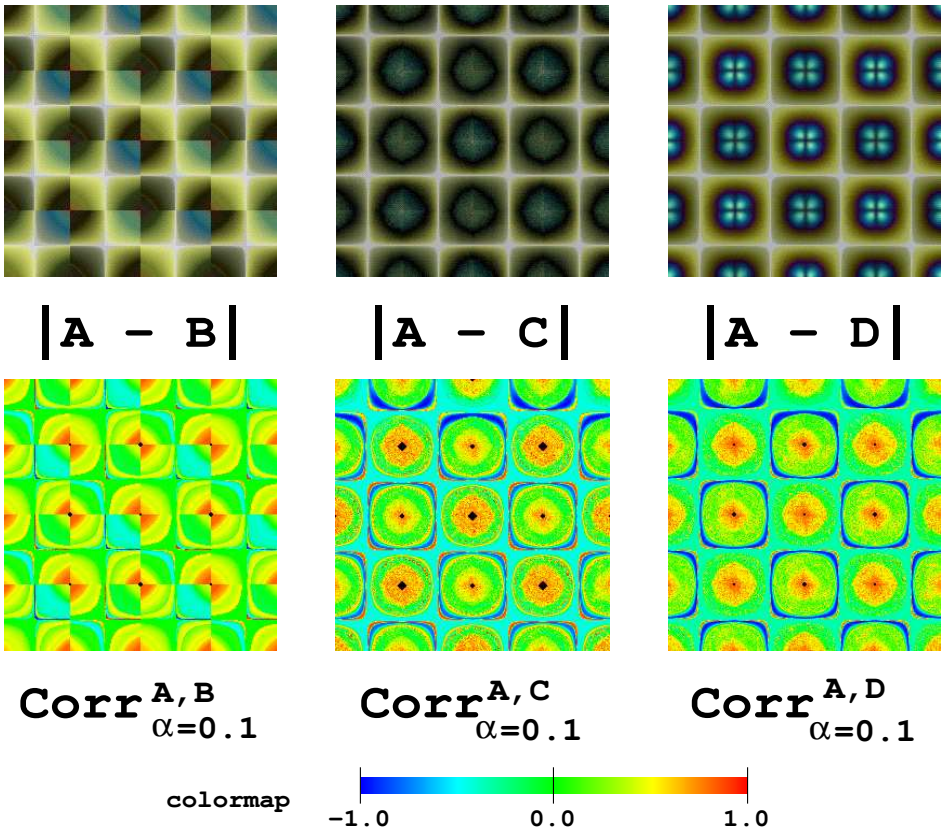

Figure 14: Difference images and visualizations of data level metrics with opacity threshold 0.1 for the images used in Figure 12. The color map given at the bottom is used for visualizing sample color correlations (Corr).

it is partially due to the material color distributions in the classification function defined in Figure 18a. However, around data points, there are less correlations in CentDiff vs InterDiff ($Corr^{A,B}_{\alpha=0.1}$) than compared to CentDiff vs other Derivative Filters. In this example, we focus on generating distinctively different patterns for each gradient calculation patterns. Note that it is generally difficult to specify a single transfer/classification function for comparing all aspects of rendering qualities. In this paper, transfer/classification functions are defined for each test data set so that certain specification variations would generate the worst cases of differences. Therefore, our test data go with different transfer functions and the image and data level comparison studies can be done accordingly.

We demonstrated how the test data sets can be used to differentiate among many specification items as well as to estimate and evaluate their differences. However, we found that it is not

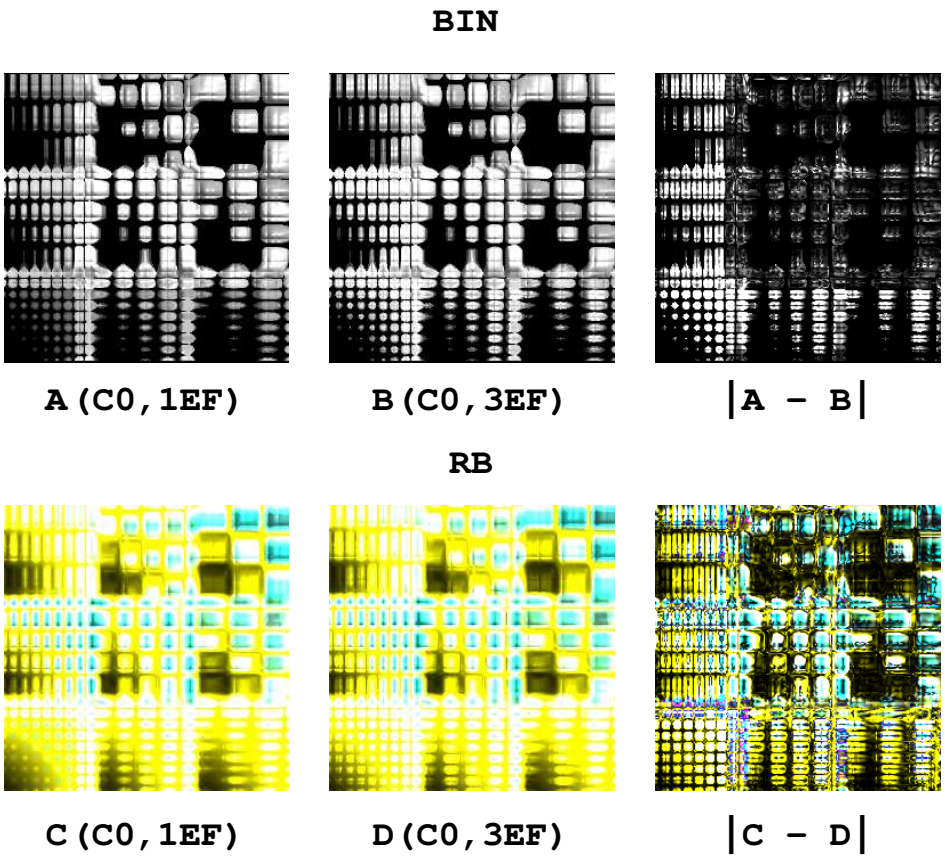

Figure 15: Differences in gradient filters. We used both Binary (for A and B) and Region Boundary (for C and D) Surface classifications.

straight-forward to generate test cases that can differentiate certain algorithm variations. For example, it is not easy to generate distinctively different images for algorithms using different gradient calculation with derivative filters given by Möller [19]. The examples shown may seem to suggest that simple datasets that highlight differences are easy to synthesize. The following example is provided to give an indication to the contrary. Using a varying frequency checker board was anticipated to be a good gradient error comparison because gradient filters have different sizes and weights. Figure 15 shows the differences in some of the derivative filters. The size of the entire data is $27 \times 27 \times 9$ and it consists of 9 sub-data blocks. Each block of data is a $9 \times 9 \times 9$ **3DCheckerBoard**. We gave different distance d and size of steps (step) to increment or decrement the data values between minimum and maximum values. Figure 16 shows a one dimensional example where $d = 6$ and two different step sizes. Details for each of the 9 sub-blocks of the data

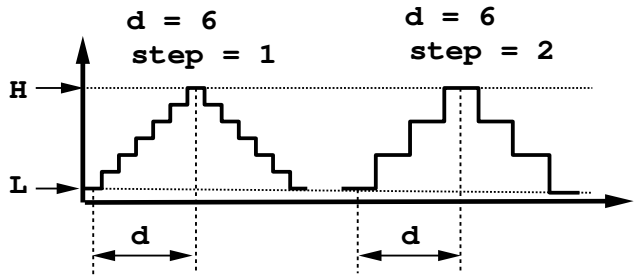

Figure 16: Effects of changing step sizes in 3DCheckerBoard.

are specified in Figure 19 of the Appendix. These variations are attempts to increase differences and generate distinctively different images for as many derivative filters as possible. However, it does not generate more or better measures than the general qualitative differences that can be assessed by Marschner and Lobb's [16] data. For general quality comparisons of new algorithm variations, some widely used standard test data (such as MRI brain) or specially designed data [16, 20, 33] have been used. In some cases, these data sets can be superior differentiators between algorithms. The advantage of our test suite is in differentiating specification items and performing detailed comparison studies of algorithms using image and data level metrics. It includes assessing differences in special or worst cases.

8 Summary

We discussed the list of important specifications for DVR algorithms. This list includes possibly subtle variations that may often be ambiguous or even ignored in the published literature in the field of volume rendering. We then presented two simple data sets that can be used for clearly identifying variations in the algorithm specifications. The datasets generate differences that make it simple to distinguish between rendering variants. This is a marked improvement over using test data, where verisimilitude is the goal, because variations are only slight and may be overlooked. We showed examples of the superiority of the checkerboard data over the commonly used MRI brain, Hipip, and Marschner and Lobb data sets. The examples demonstrate the usage of the DVR algorithm specification list and test data sets for in depth comparison studies via both image and

data level metrics. We also gave detailed specifications for our examples so that other researchers may make more quantitative comparisons of different DVR methods. Our comparison study includes assessing differences in special and worst cases for the given algorithm variations. The new datasets and metrics highlight differences between algorithms. In real datasets there will be subtle differences, but it will be hard to say what is superior. These tools make it clear why the differences exist. It is up to the developer to determine the appropriate trade-offs for their applications and datasets.

Most of the previous comparison methods use information from final rendered images only. We overcome limitations of image level comparisons with our data level approach using intermediate rendering information. We provide a list of rendering parameters and algorithm specifications to guide comparison studies. We extend Williams and Uselton's rendering parameter list with algorithm specification items and provide guidance on how to compare algorithms. Real data is often too complex to study algorithm variations with confidence. Most of the analytic test data sets reported are often useful only for a limited feature of DVR algorithms. We provide simple and easily reproducible test data sets, a checkerboard and a ramp, that can make clear differences in a wide range of algorithm variations. With data level metrics, our test data sets make it possible to perform detailed comparison studies.

Part of the results of this paper are to conclude that designing data to highlight differences is difficult. And, we found that it was not possible in some cases to generate test data that resulted in strong differences. In the beginning of this paper, we gave an overview of comparison studies in which we use the specification list and test data sets from our earlier work [8, 9]. The tools presented here can be considered as another step towards an on-going research goal of providing more standardized and objective comparison for DVR algorithms. We plan to extend and strengthen all the steps involved in the comparison process including data level metrics, test data sets, and DVR algorithm specifications.

9 Acknowledgements

We would like to thank Torsten Möller, the Client and Media Systems Laboratory of H.P. Laboratories, the members of the Advanced Visualization and Interactive Systems laboratory at UCSC, and the anonymous reviewers for their feedback and suggestions. This project is supported in part by DARPA grant N66001-97-8900, LLNL Agreement No. B347879 under DOE Contract No. W-7405-ENG-48, NSF NPACI ACI-9619020, and NASA grant NCC2-5281.

A Appendix

In this section, we provide details of the rendering parameters and algorithm specifications used to generate the images in the result section.

data	R	G	B	A
0.0	0.69	0.68	0.67	0.5
29.0	0.09	0.1	0.23	0.391
32.0	0.03	0.09	0.18	0.380
36.0	0.03	0.09	0.12	0.365
127.0	0.0	0.06	0.01	0.024
127.5	0.0	0.05	0.0	0.025
191.25	1.0	0.03	0.0	0.263
255.0	1.0	0.0	0.0	0.5

(a)

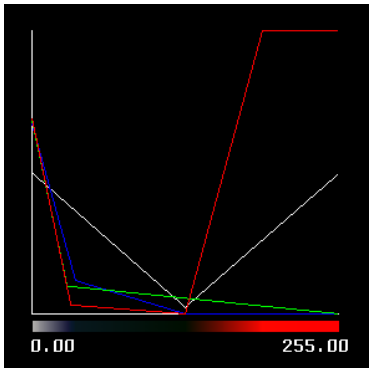

(b)

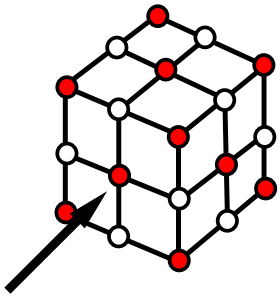

(c)

Figure 17: Transfer function table (a), diagram (b), and (c) 3^3 3DCheckerBoard data. RGBA intensities of transfer function are scaled to the range of (0, 1.0). The red sphere indicates maximum (255) and the white sphere indicates minimum (0) of the data. The arrow shows the viewing direction which is orthogonal to the front plane of the volume.

Figure 17, (a) and (b) show the transfer function for the data rendered in Figure 6 (A - E). The material color and their RGBA intensities are displayed with the color intensity graphs and their material color mapping. The opacity is displayed with the white line and the intensity of each color component is displayed by their color. The color combinations and opacity distribution for the data range have been chosen to increase differences. Figure 17b shows the data set (3DCheckerBoard) with $n = 3$ (3^3 data locations, 2^3 cells). The data range is (0, 255) and the

minimums and maximums are displayed with the white and red spheres respectively. The viewing direction is orthogonal to the front plane of the volume as indicated by the arrow in the diagram in Figure 17c.

Data Range	Color	Opacity
(127, 255)	1.0	0.45

Table 10: Binary Surface specifications for the algorithm used to generate the image A of Figure 11.

Region	f_v	α_v	Color Intensity
0	0	0.0	0
1	126	0.0	0
2	127	0.45	255
3	255	0.45	255

Table 11: Region Boundary Surface specifications for the algorithm used to generate the image B of Figure 11.

Data Range	Color	Opacity
(110, 144)	1.0	0.45

Table 12: Binary Surface specifications for the algorithm used to generate the image C of Figure 11.

f_v	r	Color	α_v
100	0.7	1.0	0.45

Table 13: Iso-value Contour Surface specifications for the algorithm used to generate the image D of Figure 11.

In order to specify Iso-value Contour and Region Boundary Surface classifications, we give coefficients for the formula defined in Levoy [13]. For Iso-value Contour Surfaces, we give the iso-value (f_v) for the surface, its opacity (α_v) and the transition region thickness r. For Region Boundary Surfaces, we give the data values of region boundaries (f_v), its opacity (α_v) and its color intensities. We also give a function table that maps the given gradient magnitude to a value to be multiplied to the color(or opacity) values resulted from the classification function [13]. Table 10 to Table 13 provide the surface classification definitions for the algorithm used in Figure 11 (A - D). We gave the data range and color intensity for Binary Surface classification. All renderings were done in grey scale for this example. Similar definitions are given for the example of gradient calculations (Figure 12). The material color is given in Figure 18a and its Region Boundary Surface specifications are given in Figure 18b. We used a linear function (given in Figure 18c) that scales gradient magnitudes before multiplying with the α_v opacity values from the Region Boundary Surface classification.

The block diagram and details for the data used in Figure 15 are given in Figure 19. The block number in the diagram corresponds to each block in images of Figure 15. For each block, the half

(a)

Region	f_v	α_v	R	G	B
0	0	0.05	0.7	0.0	0.0
1	126	0.35	1.0	1.0	0.0
2	127	0.45	1.0	1.0	1.0
3	174	0.35	0.0	1.0	1.0
4	255	0.05	0.7	0.0	0.0

(b)

$\lvert\nabla f(x)\rvert$	value
0	0.1
5	0.9
100	1.0
254	1.0

(c)

Figure 18: (a) Material color band, (b) Region Boundary Surface specifications, and (c) gradient magnitude scaling function used to generate the images of Figure 12.

frequency sizes and the step sizes are given in each dimension.

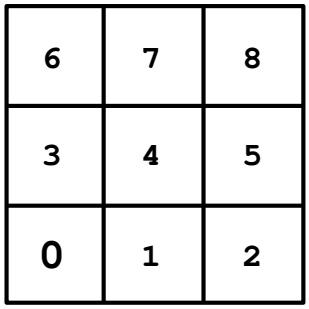

block no.	x		y		z	
	d	step	d	step	d	step
0	1	1	1	1	1	1
1	2	1	1	1	2	1
2	3	1	1	1	3	1
3	1	1	2	2	2	2
4	2	1	2	2	2	2
5	3	2	2	2	3	2
6	1	1	3	3	3	1
7	2	2	3	1	3	2
8	3	3	3	2	3	3

Figure 19: Step distance and size of each block of 3DCheckerBoard data used in Figure 15. The data is $27 \times 27 \times 9$ and is subdivided into 9 sub-blocks, each of which is $9 \times 9 \times 9$.

References

[1] J. Arvo and K. Novins. Iso-contour volume rendering. In *Proceedings 1994 Symposium on Volume Visualization*, pages 115–122. IEEE, October 1995.

[2] Mark J. Bentum, Barthold B.A. Lichtenbelt, and Thomas Malzbender. Frequency analysis of gradient estimators in volume rendering. *IEEE Transactions on Visualization and Computer Graphics*, 2(3):242–254, September 1996.

[3] Brian Cabral, Nancy Cam, and Jim Foran. Accelerated volume rendering and tomographic reconstruction using texture mapping hardware. In *Proceedings 1994 Symposium on Volume Visualization*, pages 91–98, Washington, D.C., Oct 1994. IEEE/ACM.

[4] R. A. Drebin, L. Carpenter, and P. Hanrahan. Volume rendering. In *Proceedings of SIGGRAPH 88*, pages 65–74, August 1988.

[5] Ajeetkumar Gaddipatti, Raghu Machiraju, and Roni Yagel. Steering image generation with wavelet based perceptual metric. *Computer Graphics Forum*, 16(3):C241–251, C391, September 1997.

[6] A. Globus and S. Uselton. Evaluation of visualization software. *Computer Graphics*, pages 41–44, May 1995.

[7] M.E. Goss. An adjustable gradient filter for volume visualization image enhancement. In *Proceedings Graphics Interface*, pages 67–74, 1994.

[8] Kwansik Kim and Alex Pang. A methodology for comparing direct volume rendering algorithms using a projection-based data level approach. In *Eurographics/IEEE TVCG Symposium on Visualization*, pages 87–98, Vienna, Austria, May 1999.

[9] Kwansik Kim and Alex Pang. Ray-based data level comparisons of direct volume rendering algorithms. In Hans Hagen, Gregory Nielson, and Frits Post, editors, *Scientific Visualization, Dagstuhl'97 Workshop Proceedings*, pages 137–150, 347. IEEE Computer Society, 1999.

[10] George Klir and Mark Wierman. *Uncertainty-Based Information: Elements of Generalized Information Theory, 2nd edition*. Physica-Verlag, 1999. 168pp.

[11] Philippe Lacroute and Marc Levoy. Fast volume rendering using a shear-warp factorization of the viewing transformation. In *Proceedings of SIGGRAPH 94*, pages 451–458, Orlando, FL, July 1994.

[12] David Laur and Pat Hanrahan. Hierarchical splatting: A progressive refinement algorithm for volume rendering. In *Proceedings of SIGGRAPH 91*, volume 25, pages 285–288, July 1991.

[13] Marc Levoy. Display of surfaces from volume data. *IEEE Computer Graphics and Applications*, 8(5):29–37, May 1988.

[14] R. Machiraju and R. Yagel. Reconstruction error characterization and control: A sampling theory approach. *IEEE Transactions on Visualization and Computer Graphics*, pages 364–378, December 1996.

[15] Tom Malzbender. Fourier volume rendering. *ACM Transactions on Graphics*, 12(3):233–250, July 1993.

[16] S. R. Marschner and R. J. Lobb. An evaluation of reconstruction filters for volume rendering. In *Proceedings of Visualization*, pages 100–107. IEEE, October 1994.

[17] Nelson Max. Optical models for direct volume rendering. *IEEE Transactions on Visualization and Computer Graphics*, 1(2):99–108, June 1995.

[18] Torsten Möller, Raghu Machiraju, Klaus Müller, and Roni Yagel. A comparison of normal estimation schemes. In *Proceedings of the IEEE Conference on Visualization 1997*, pages 19–26, October 1997.

[19] Torsten Möller, Klaus Müller, Yair Kurzion, Raghu Machiraju, and Roni Yagel. Design of accurate and smooth filters for function and derivative reconstruction. In *Proceedings of the 1998 Symposium on Volume Visualization*, pages 143–151, October 1998.

[20] Ulrich Neumann. *Volume Reconstruction and Parallel Rendering Algorithms: A Comparative Analysis*. PhD thesis, UNC, Chapel Hill, 1993.

[21] Hans-Georg Pagendarm and Frits H. Post. Studies in comparative visualization of flow features. In G. Nielson, H. Hagen, and H. Muller, editors, *Scientific Visualization: Overviews, Methodologies, Techniques*, pages 211–227. IEEE Computer Society, 1997.

[22] A. Pang, C.M. Wittenbrink, and S. K. Lodha. Approaches to uncertainty visualization. *The Visual Computer*, 13(8):370–390, 1997.

[23] Nivedita Sahasrabudhe, John E. West, Raghu Machiraju, and Mark Janus. Structured spatial domain image and data comparison metrics. In *Proceedings of Visualization 99*, pages 97–104,515, 1999.

[24] U. Tiede, K.H. Hohne, M. Bomans, A. Pommert, M. Riemer, and G. Wiebecke. Surface rendering: Investigation of medical 3D-rendering algorithms. *IEEE Computer Graphics and Applications*, 10(2):41–53, March 1990.

[25] Allen Van Gelder and Kwansik Kim. Direct volume rendering with shading via 3D textures. In *ACM/IEEE Symposium on Volume Visualization*, pages 22–30, San Francisco, CA, October 1996.

[26] J. Terwisscha van Scheltinga, M.K. Bosma, J. Smit, and S. Lobregt. Image quality improvements in volume rendering. In *Lecture notes in computer science, (Fourth International Conference on Visualization in Biomedical Computing) VBC '96*, volume 1131, pages 87–92. Springer-Verlag, September 1996.

[27] L. Westover. Footprint evaluation for volume rendering. In *Proceedings of SIGGRAPH 90*, pages 367–376, August 1990.

[28] Lee A. Westover. *Splatting: A Parallel, Feed-Forward Volume Rendering Algorithm*. PhD thesis, University of North Carolina at Chapel Hill, 1991.

[29] Jane Wilhelms and Allen Van Gelder. A coherent projection approach for direct volume rendering. In *Proceedings of SIGGRAPH 91*, pages 275–284, 1991.

[30] Peter L. Williams and Nelson L. Max. A volume density optical model. In *Proceedings of 1992 Workshop on Volume Visualization*, pages 61–68, Boston, October 1992.

[31] Peter L. Williams and Samuel P. Uselton. Metrics and generation specifications for comparing volume-rendered images. *The Journal of Visualization and Computer Animation*, 10:159–178, 1999.

[32] Craig M. Wittenbrink, Thomas Malzbender, and Michael E. Goss. Opacity-weighted color interpolation for volume sampling. In *Proceedings of the 1998 Symposium on Volume Visualization*, pages 135–142, color plate page 177, October 1998. Also available as Technical Report, HPL-97-31R2, Hewlett-Packard Laboratories, Palo Alto, CA, Revised Apr. 1998.

[33] Craig M. Wittenbrink and A. K. Somani. Time and space optimal parallel volume rendering using permutation warping. *Journal of Parallel and Distributed Computing*, 46(2):148–164, November 1997.